

Shared Cross-Modal Trajectory Prediction for Autonomous Driving

Chiho Choi

Honda Research Institute USA
cchoi@honda-ri.com

Abstract. We propose a framework for predicting future trajectories of traffic agents in highly interactive environments. On the basis of the fact that autonomous driving vehicles are equipped with various types of sensors (*e.g.*, LiDAR scanner, RGB camera, etc.), our work aims to get benefit from the use of multiple input modalities that are complementary to each other. The proposed approach is composed of two stages. (i) *feature encoding* where we discover motion behavior of the target agent with respect to other directly and indirectly observable influences. We extract such behaviors from multiple perspectives such as in top-down and frontal view. (ii) *cross-modal embedding* where we embed a set of learned behavior representations into a single cross-modal latent space. We construct a generative model and formulate the objective functions with an additional regularizer specifically designed for future prediction. An extensive evaluation is conducted to show the efficacy of the proposed framework using two benchmark driving datasets.

Keywords: Trajectory prediction, Future vehicle/pedestrian localization, Generative method, Cross-modal embedding, Autonomous driving

1 Introduction

Recent advances in scene understanding have enabled machines to acquire knowledge of the surrounding environment. This rapid progress particularly in object detection [1,2,3], tracking [4,5,6], and semantic segmentation [7,8,9] made within the last few years raises expectations about the emergence of autonomous vehicles. Based upon the success use of visual understanding for driving, the safe operation of vehicles has become the next central challenge to remove humans from behind the steering wheel. To succeed in safe driving, the driving models should consider the past behavior of interactive agents (*i.e.*, pedestrians, cars, cyclists, etc.) and predict the future motion of whom share roads with them.

Intensive research has been conducted on forecasting future motion of humans and that of vehicles. However, current existing approaches may not be suitable for general-purpose trajectory forecast in traffic scenes because of the following reasons: (i) social interactions are validated from the *nearby* surroundings with an assumption of slow movement of agents (*i.e.*, pedestrians) [10,11], which is not generally applicable to vehicles as they move faster; (ii) the interactive environment is hypothesized as an open space, resulting in no or minimal considerations

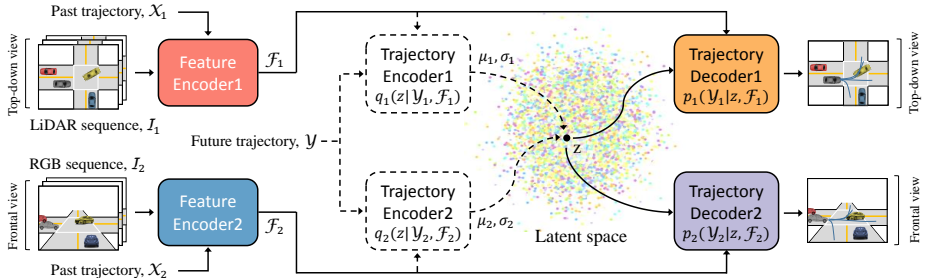


Fig. 1: Given a sequence of images and past positions, the feature encoder analyzes internal, external, and social stimuli of agents. The features generated from multiple sensory data (e.g., top-down view LiDAR and frontal view RGB) are used to condition the generative model that aims to embed different input modalities into a single cross-modal latent space. The following decoder predicts future trajectory in top-down or frontal view using the latent variable sampled from the learned embedding space. Note that the dotted shapes and arrows are only visible at training time.

of scene context [12,13,14,15,16,17], which is not a feasible assumption in traffic scenes with structured layouts; (iii) the proposed solutions are restricted to certain scenarios (e.g., highway in [18,19] or ego-future in [20,21,22,23]) and not generalizable to other settings; and (iv) vehicle interactions with pedestrians are overlooked [24,25,26,27,28,29], which is essential for the safe operation of vehicles with driving automation systems. Therefore, a robust solution for trajectory prediction in traffic scenes still does not exist.

In this view, we introduce a framework that addresses the aforementioned issues for predicting future trajectories of road agents in highly interactive environments. An overview of the proposed approach is illustrated in Fig. 1. The first part of the system (as detailed in Fig. 2) determines motion behavior of the target agent with respect to other directly and indirectly observable influences. We borrow the notion of *stimuli* in [30] to categorize such influences into three types as in [31]. *Inertial stimuli* find motion intent of the target agent by observing the sequence of its past state such as positions. We explicitly model the motion history of the target by implicitly considering its local perceptions. *Environmental stimuli* include contextual cues of the surroundings such as road topology, geometry, and semantic information. We encode both spatial and temporal attributes of the environment from the past image sequence. *Social stimuli* consider relational interactions between the target agent and all other traffic participants. We infer pair-wise relations to model the social behavior from interactive agents. Note that the proposed feature encoder is not specifically designed for a certain type of input but commonly used for any modalities of sensory data (e.g., top-down view LiDAR, frontal view RGB, etc.). As shown in Fig. 1, we extract such stimuli from two exemplary input modalities.

The second part of the system aims to get benefit from the use of multiple input modalities that are complementary to each other. For this, we embed the encoded stimuli extracted from individual sensor modes into a single shared latent space. Our conditional variational autoencoder (CVAE)-based generative models jointly optimize the objective functions across different input modalities, so that the descriptions about the same scenario from different perspectives can get closer to each other in the embedding space. The latent variables sampled from this space can generate future trajectories both in top-down and frontal view through the following decoders conditioned on the encoded motion behavior. To the best of our knowledge, we are the first to investigate multiple input/output modalities from a single framework with the aim of general-purpose trajectory prediction, unlike the separation of the existing works in top-down view for autonomous driving [11,24,25] and in frontal view for advanced driver assistance systems (ADAS) [32,21,23].

To this end, we generate multiple modes of future trajectory by sampling the latent variables from the learned cross-modal space. However, this random sampling-based strategy [11,25] likely predicts similar trajectories, ignoring the random variable input while generating output from the decoder. This posterior collapse¹ problem of VAE and its variants is particularly critical to future prediction as it mitigates the multi-modality of the system. Therefore, we design a regularizer (i) that pushes the model to rely on the latent variables to predict diverse modes of future motion and (ii) that does not weaken the prediction capability of the decoder while preventing the performance degradation.

The main contributions of this paper are summarized as follows:

1. Motion behavior of the agent is encoded from directly and indirectly observable influences, in the form of inertial, environmental, and social stimuli.
2. A single structure of feature extractor is designed to encode such stimuli, which is applicable to any modalities of sensory data.
3. Shared cross-modal embedding is introduced to get benefit from different types of input modalities that are complementary to each other.
4. A regularizer is specifically designed for future prediction to mitigate posterior collapse of CVAE and to predict more diverse modes of motion behavior.

Throughout the paper, we use the word ‘multi-modality’ to denote two different sources. First, *multi-modal input* represents input data obtained from different types of sensors such as LiDAR scanner and RGB camera. Second, *multi-modal prediction* depicts predicted trajectory outputs with multiple variations.

2 Related Work

In this section, we review the deep learning-based approaches that are most relevant to the proposed framework.

¹ We do not carry out any study on mode collapse of GANs or related problems other than posterior collapse of VAEs where our structure is built on.

Trajectory Prediction in Crowds In the last years, a majority of research on trajectory prediction [10,13,15,33] has been conducted toward modeling the interactive behavior between humans. These works first use the recurrent operation of neural networks to encode the temporal information using individual humans’ motion sequence. Then, a correlation between encoded features is found through the explicit social module. Recently, social interactions have been modeled using the edges of the graph structure in [16]. Although these methods may be successful in interaction modeling, they overlook the environmental influences that may cause prediction failure in structured environments. Therefore, the subsequent works in [11,34,35] take images as input to constrain their prediction model using scene context. [36] finds both social and environmental interactions by implicitly analyzing the relations between sub-regions of images. Inspired by their implicit modeling of relations, we design a new interaction encoder that explicitly captures the relational behavior of individual entities.

Vehicle Trajectory Prediction in Top-down View Similar interaction modules are applied for vehicle trajectory prediction in driving scenarios. Some approaches only consider the past motion of road agents [18,19,17,37], and thus result in large errors with a complex road environment. To alleviate such problems, [24,38,25,28] input visual information as an additional cue to condition their model on the road topology. However, they overlook the vehicle interactions against pedestrians, which is most critical to model the natural behavior of vehicles on the road for safe driving. Unlike these methods, we do not limit our scope to ‘vehicle’ trajectories and its interactions. Our framework is a more general solution in traffic scenes in the sense that we forecast future trajectories of any agents by discovering the interactions of the target with all other agents.

Vehicle Trajectory Prediction in Frontal View [32,21,23] aim to predict the future trajectory of vehicles in a frontal view image space. They predict a target agent’s *relative* trajectory with respect to the potential motion of ego-vehicle. Therefore, the prediction outcomes are valid only if the accurate ego-future is available. In practice, however, prediction of ego-motion is an another research topic [22] in the transportation domain, which makes hard to apply such systems into the real world applications. Therefore, we predict the *absolute* coordinates of trajectories with ego-motion compensation in frontal view.

Multi-Modal Learning Learning representations of multiple input modalities have been explored in recent years. As described in [39], multi-modal learning can be categorized into three types. *Multi-modal fusion* takes multiple modalities as input and learns their joint representations. Basically, the same set of input types should be provided at test time as in [40,41]. *Cross-modal learning* tries to learn more descriptive representations from one modality when auxiliary modalities are given at training time. During inference, the auxiliary modalities are not necessary as in [42,43]. *Shared representation learning* learns the representation from one modality and performs the test on the other modality as shown in [44,45]. The proposed cross-modal embedding aligns in between cross-modal learning and shared representation learning, similar in spirit to [46]. We aim to benefit from different modalities that are correlated to each other. How-

ever, rather than learning common representations, we try to embed different representations into the shared cross-modal latent space.

3 Preliminaries

3.1 Input Modality

In this paper, multiple sensory data is used as input to the proposed framework. We use two exemplary data types that can be easily accessible in the benchmark driving datasets: (i) *LiDAR data* provide 3D scanning of the surrounding environments. Using the 3D point clouds, we project every single point in top-down view and predict trajectories of traffic agents in the world coordinates. (ii) *RGB images* captured from a frontal-facing camera provide rich and dense representations. We predict the trajectories from the egocentric perspective in the image space, following the literature [20,21]. However, the predicted trajectories are the absolute locations with respect to the first observation frame, eliminating the effect of future motion of ego-vehicle².

Note that the input modalities are not limited to these two types but also include stereo images, depth, radar, GPS, and many others that can provide visual/locational information.

3.2 Problem Formulation

Given the motion history of traffic agents and corresponding image sequence, we predict the target agent’s future trajectory in driving scenes. During τ number of the observation time steps, the optical flow $\mathcal{O} = \{O_{t_0-\tau+2}, O_{t_0-\tau+3}, \dots, O_{t_0}\}$ and segmentation map S is computed using sensor data $\mathcal{I} = \{I_{t_0-\tau+1}, I_{t_0-\tau+2}, \dots, I_{t_0}\}$. Note that we do not distinguish the notations of two different sensor modalities unless otherwise mentioned. In addition, we assume that the coordinates of K traffic agents $X = \{\mathcal{X}^1, \mathcal{X}^2, \dots, \mathcal{X}^K\}$ are available with a same coordinate with \mathcal{I} , where $\mathcal{X} = \{X_{t_0-\tau+1}, X_{t_0-\tau+2}, \dots, X_{t_0}\}$ with $X = (x, y)$. Given $\{\mathcal{O}, S\}$ and X , we first extract the feature representation \mathcal{F} that is composed of three stimuli. Then, the encoder $Q(z|\mathcal{Y}, \mathcal{F})$ embeds \mathcal{F} into the latent space. The following decoder $P(\mathcal{Y}|z, \mathcal{F})$ finds the future locations $\mathcal{Y}^k = \{Y_{t_0+1}^k, Y_{t_0+2}^k, \dots, Y_{t_0+\delta}^k\}$ of the target agent k using the latent sample z , where the prediction time horizon is defined by δ .

4 Methodology

4.1 Feature Encoding

We describe the proposed feature extractor that models motion behavior of the target agent with respect to other directly and indirectly observable influences.

² In the supplementary material, we describe the data preparation in detail.

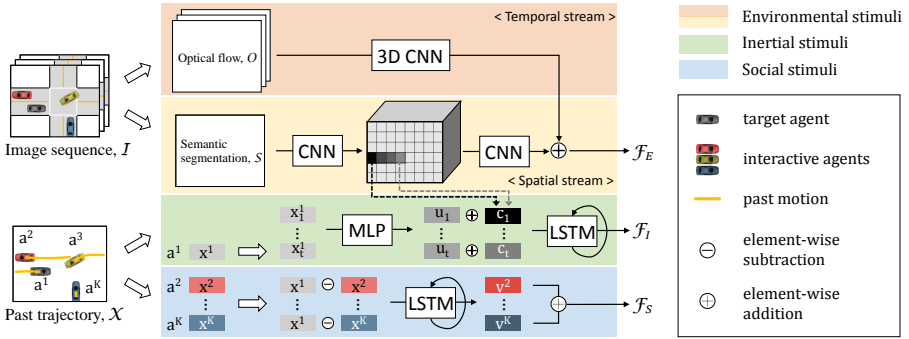


Fig. 2: The detailed illustration of the proposed feature encoder. Using the past image sequence, we model spatio-temporal factors given by external environments. The internal factors of the target agent is encoded from its past motion as well as surrounding local perceptual context. In addition, we consider the relative motion between the target and every other interactive agents to construct the social interactions.

Environmental Stimuli The importance of external constraints on trajectory prediction is particularly pronounced for traffic agents in driving scenes. To model such environmental influences, the system should be able to recognize each object’s static/dynamic states as well as the semantic context of the scene. In this view, we respectively construct a two-stream network – temporal stream and spatial stream – as shown in Fig. 2 (orange and yellow box).

The image sequence \mathcal{I} captured during the past time steps is used to generate two types of representations: a set of optical flow images \mathcal{O} and a segmentation map \mathcal{S} . The optical flow is computed with a TV-L1 [47] algorithm, containing the pattern of objects’ motion. The temporal changes of the objects are processed using the 3D convolutional neural network $CNN_{3D}(\cdot)$ by extracting temporal representations \mathcal{F}_T along the time axis.

$$\mathcal{F}_T = CNN_{3D}(\mathcal{O}; W_T), \quad (1)$$

where W_T is the learned weight parameters.

In addition, a pixel-level segmentation map is obtained for each image at the first time step. We run the DeepLab-V2 model [9] trained on the Cityscapes dataset [48]. Among the estimated labels, we only leave the background structures such as road, sidewalk, vegetation, etc. to extract visual features from the stationary environment. The 2D convolutional neural network $CNN_{2D}(\cdot)$ is used in this stream to take advantage of its spatial feature encoding.

$$\mathcal{F}_V = CNN_{2D}(\mathcal{S}; W_V), \quad (2)$$

where W_V is the learned weight parameters.

We merge the temporal states \mathcal{F}_T of static/dynamic objects and the spatial features \mathcal{F}_V of the stationary context to generate spatio-temporal features \mathcal{F}_E given as follows:

$$\mathcal{F}_E = \mathcal{F}_T \oplus \mathcal{F}_V, \quad (3)$$

where \oplus is an element-wise addition operator.

Inertial Stimuli Each road agent has its own intent to make a certain motion behavior based on the past states. We find such agent-centric motion intent for the target agent k , performing the following procedure. Given the observation time horizon and the target agent index k , we encode its past locations \mathcal{X}^k into high dimensional feature representations \mathcal{U}^k through the multi-layer perceptron (MLP). The encoded features are then combined with the local perception that contains mid-level semantic context C_{X_t} (nearby areas of X_t at time t). By adding spatial locality, interactions of the target toward the local environments further constrain the motion intent of the target. The following LSTM captures the temporal dependency of the motion states on the local environments by

$$\begin{aligned} \mathcal{U}_t^k &= MLP_I(\mathcal{X}_t^k; W_E), \\ h_{I,t+1} &= LSTM_I(\mathcal{U}_t^k \oplus C_{X_t}, h_{I,t}; W_I), \end{aligned} \quad (4)$$

where W_E and W_I is the learnable parameters of MLP and LSTM layer and $h_{I,t}$ denotes the hidden state of the LSTM encoder at time t . These steps are illustrated in Fig. 2 (green box). We define the last hidden state of LSTM as \mathcal{F}_I .

Social Stimuli We model the social behavior between interactive agents with their pair-wise relations. We first compute the relative motions of all road agents with respect to the motion of the target k for the past time steps. Each agent's relative motion is processed through LSTM, encoding the relational behavior between the target and every individuals.

$$\begin{aligned} \mathcal{V}^i &= \mathcal{X}^k \ominus \mathcal{X}^i \quad \forall i \in \{1, \dots, K\} \setminus \{k\}, \\ h_{S,t+1} &= LSTM_S(\mathcal{V}_t^i, h_{S,t}; W_S), \end{aligned} \quad (5)$$

where W_S is the learnable parameters of LSTM, $h_{S,t}$ denotes the hidden state of the LSTM encoder at time t , and \ominus is an element-wise subtraction operator. This process is simple yet effective to infer temporal changes of interactive behavior between every pairs of agents. We use the last hidden state of each agent $i \in \{1, \dots, K\} \setminus \{k\}$ as \mathcal{F}_S^i . The resulting feature representations \mathcal{F}_S^i of individual agents are then combined as social features \mathcal{F}_S given by

$$\mathcal{F}_S = \sum_i \mathcal{F}_S^i \quad \forall i \in \{1, \dots, K\} \setminus \{k\}. \quad (6)$$

See Fig. 2 (blue box) for the visualization of this process.

We further aggregate environmental representations $\mathcal{F}_E \in \mathbb{R}^{d \times d \times c}$ with social representations $\mathcal{F}_S \in \mathbb{R}^{1 \times 1 \times c}$, where d denotes the width/height of the feature

and c is its depth. For this, we generate an empty tensor $\mathcal{F}_X \in \mathbb{R}^{d \times d \times c}$ that has a same shape with \mathcal{F}_E and fill the elements using \mathcal{F}_S based on the location $X_{t_0}^k$ of the target at time t_0 . The produced features contain the spatio-temporal influences of all external factors toward the target agent, which explicitly constrain its future motion on interactions. We further construct pair-wise relations between entities of \mathcal{F}_X by conditioning on the inertial representations \mathcal{F}_I , similarly to [36]:

$$\mathcal{F} = \sum_{i,j} MLP_A(\mathcal{F}_{X,i}, \mathcal{F}_{X,j}, \mathcal{F}_I; W_A), \quad (7)$$

where $i, j \in \{1, \dots, d\}$ and W_A is the learnable weight parameters.

4.2 Shared Cross-Modal Embedding

The CVAE framework has been widely used in the literature due to its generative modeling capability with high reconstruction accuracy. Such benefits come from maximizing the variational lower bound on the log-likelihood, which can be written as follows:

$$\log P(\mathcal{Y}|\mathcal{F}) \geq -KL(Q(z|\mathcal{Y}, \mathcal{F})\|P(z|\mathcal{F})) + \mathbb{E}_{Q(z|\mathcal{Y}, \mathcal{F})}[\log P(\mathcal{Y}|z, \mathcal{F})], \quad (8)$$

where $Q(z|\mathcal{Y}, \mathcal{F})$ and $P(\mathcal{Y}|z, \mathcal{F})$ respectively denotes an encoder and decoder, \mathcal{F} is a condition, and z is a latent variable. The network parameters of the encoder are learned to minimize the Kullback-Leibler divergence between the prior distribution $P(z|\mathcal{F})$ and its approximation $Q(z|\mathcal{Y}, \mathcal{F})$. The second term is the log-likelihood of samples, which is considered as the reconstruction loss of the decoder.

We reformulate the CVAE framework to embed multiple input modalities in the shared latent space. Assuming that different data types $\{\mathcal{I}, X\}_i$ are available (e.g., $i \in \{LiDAR, RGB\}$), the proposed method predicts future trajectory \mathcal{Y}_i of the target agent with the same modalities i . In the mean time, the encoders learn to embed feature representations \mathcal{F}_{LiDAR} and \mathcal{F}_{RGB} as close as possible in the embedding space. The decoders generate trajectories using the same latent variable z sampled from the prior that is modeled as Gaussian distribution $z \sim \mathcal{N}(0, I)$. In this sense, the objective function becomes as follows:

$$\mathcal{L}_E = \sum_i (-KL(Q_i(z|\mathcal{Y}_i, \mathcal{F}_i)\|P_i(z|\mathcal{F}_i)) + \mathbb{E}_{Q_i(z|\mathcal{Y}_i, \mathcal{F}_i)}[\log P_i(\mathcal{Y}_i|z, \mathcal{F}_i)]), \quad (9)$$

where $i \in \{LiDAR, RGB\}$ indicates different types of modalities, $Q_i(\cdot)$ and $P_i(\cdot)$ is an encoder-decoder pair of each modality.

4.3 Multi-modal Prediction

In practice, the optimization of CVAE is challenging itself because of the posterior collapse problem. The strong autoregressive power of the decoder often ignores the random variable z sampled from the learned latent space. Thus, the

output is dominantly generated using the conditional input \mathcal{F} , still satisfying the minimization of the KL divergence and maximization of the log-likelihood in Eqn. 8. Such a problem alleviates the multi-modal nature of future prediction where multiple plausible trajectories are generated given the same past motion.

While tackling posterior collapse, we aim to address the following challenges: (i) our technique helps to generate diverse responses from the decoder, which enables multi-modal prediction and (ii) it does not physically weaken the decoder to alleviate its prediction capability while preventing the performance degradation. In this sense, we introduce an auxiliary regularizer in the loss function, which pushes the decoder to rely on the latent variable.

At training time, we assume that there exist N modes of trajectories for each query. Then, the latent variables $z_i \sim Q(z_i|\mathcal{Y}, \mathcal{F}) = \mathcal{N}(\mu, \sigma^2)$ are sampled from the normal distribution of the encoder with the mean μ and variance σ^2 , where $i \in \{1, \dots, N\}$. We consider the trajectories generated using these latent variables as N modes of predictions. To maximize the physical distance between each pair of modes, their pair-wise similarity is evaluated using Gaussian kernel by

$$K(\mathcal{Y}_i, \mathcal{Y}_j) = \exp\left(-\frac{D(\mathcal{Y}_i, \mathcal{Y}_j)}{2\sigma_G^2}\right), \quad (10)$$

where $D(\cdot)$ is a distance measure between trajectories \mathcal{Y}_i and \mathcal{Y}_j with $i, j \in \{1, \dots, N\}$ and σ_G^2 is the hyper-parameter of this kernel function. The regularizer is found with a pair of maximum similarity $K(\mathcal{Y}_k, \mathcal{Y}_l)$, and we train the network to minimize the similarity. This technique enforces the model to (i) actually use N latent variables while predicting output trajectories with multiple modes and (ii) minimize the similarity between predicted trajectories through the optimization without losing the prediction capability of the decoder.

As a result, the total objective function of the proposed approach is drawn as follows:

$$\mathcal{L}_{Total} = -\mathcal{L}_E + \lambda \sum_i K(\mathcal{Y}_k, \mathcal{Y}_l), \quad (11)$$

where $i \in \{LiDAR, RGB\}$ is an indicator of input sensor types and λ balances multi-modality and accuracy ($\lambda = 10$ is used). To optimize the first term in Eqn. 11, we find the trajectory \mathcal{Y}_n of the mode n that shows the maximum similarity with the ground truth. In this way, the log-likelihood in Eqn. 9 encourage the decoder to generate accurate results.

5 Experiments

We conduct evaluations using the benchmark driving datasets to validate the efficacy of the proposed approach.

5.1 Datasets and Evaluation Metrics

Datasets We use two benchmark driving datasets (KITTI [49] and H3D [6]) to evaluate the proposed approach comparing to self-generated baselines and

state-of-the-art methods. The KITTI dataset was introduced for trajectory forecast in [11] to predict future motions of road agents in top-down view, and then [21] found their future locations in frontal view using this dataset. As proposed in [11], we generate a set of trajectory segments with 6 *seconds* long (2 *sec* for observation and 4 *sec* for prediction) using Road and City scenes in the Raw subset. We split all videos into five sets and conduct 5-fold cross validation. In addition, we use the H3D [6] driving dataset that provides LiDAR scanning, frontal view RGB images, GPS/IMU, and labels of traffic agents including detection and tracking in both 2D and 3D, similar to KITTI. We further validate our approach using H3D on heterogeneous agents in highly congested urban environments. For evaluation, we divide 160 scenarios of H3D into train set (75%) and test set (25%).

Metrics For the performance comparison, we follow the standard evaluation metrics, ADE and FDE. The ADE is the average distance error computed using L2 distance between the predicted trajectory and the ground truth for a certain time duration. The FDE is the final distance error, which shows L2 distance between the predicted location and the ground truth at a certain time step. We report error rates using both metrics with 1 *sec* interval at future time steps. For multi-modal prediction, we predict $N = 10$ future trajectories and find a trajectory that shows a minimum ADE at 4 *sec* in future.

5.2 Ablative Study

We demonstrate the rationale of using the proposed approach for trajectory forecast. Note that the evaluations are conducted in top-down view using KITTI while predicting a single-modal output. We define five baseline models as follows:

1. **w/o social & env.** that only considers inertial stimuli & drive the motion of traffic agents;
2. **w/o social** where the model overlooks social influences while inertial and environmental stimuli are available;
3. **w/o spatial** where we remove the spatial stream (information about stationary structures);
4. **w/o temporal** where the temporal changes of static/dynamic objects are not considered; and
5. **w/o cross-modal** that includes all types of stimuli.

Note that these baseline models are not trained with cross-modal embedding. We thus highlight its efficacy by comparing the 5th baseline model (**w/o cross-modal**) with Ours (**Cross-modal_single** where we train the model by embedding). Table 1 shows their error rates. When one or more of stimuli is missing, a significant performance drop is observed. The error rate of the **w/o social & env.** model is particularly larger than others by a huge margin. By considering additional environmental influences (**w/o social**), the performance improves for long-term prediction toward 4*sec*. It clearly demonstrates the effectiveness of the environmental constraints. Although the error rates of **w/o spatial** and **w/o**

Table 1: Quantitative comparison (ADE / FDE in *meters*) of our approach with the self-generated baselines as well as state-of-the-art methods [10,11,13,50,36]. The KITTI dataset [51] is used to predict trajectories in top-down view.

Single-modal prediction				
Method	1.0 <i>sec</i>	2.0 <i>sec</i>	3.0 <i>sec</i>	4.0 <i>sec</i>
<i>Self-generated baselines</i>				
w/o social & env.	0.37 / 0.64	0.69 / 1.47	1.20 / 3.01	1.94 / 5.32
w/o social	0.38 / 0.65	0.68 / 1.39	1.16 / 2.96	1.87 / 4.97
w/o spatial	0.31 / 0.52	0.55 / 1.19	0.99 / 2.60	1.66 / 4.75
w/o temporal	0.31 / 0.53	0.59 / 1.27	1.05 / 2.75	1.75 / 4.88
w/o cross-modal	0.31 / 0.51	0.53 / 1.07	0.92 / 2.36	1.53 / 4.35
<i>Ours</i>				
Cross-modal_single	0.20 / 0.36	0.42 / 1.00	0.82 / 2.29	1.44 / 4.33
<i>State-of-the-art methods</i>				
Const-Vel [50]	0.34 / 0.56	0.85 / 1.79	1.60 / 3.72	2.55 / 6.24
Social-LSTM [10]	0.53 / 1.07	1.05 / 2.10	1.93 / 3.26	2.91 / 5.47
DESIRE [11]	- / 0.51	- / 1.44	- / 2.76	- / 4.45
Social-GAN [13]	0.36 / 0.54	0.76 / 1.53	1.39 / 3.21	2.25 / 5.59
Gated-RN [36]	0.34 / 0.62	0.70 / 1.72	1.30 / 3.34	2.09 / 5.55
Multi-modal prediction				
Method	1.0 <i>sec</i>	2.0 <i>sec</i>	3.0 <i>sec</i>	4.0 <i>sec</i>
<i>Ours</i>				
Cross-modal w/o reg	0.20 / 0.35	0.40 / 0.96	0.77/ 2.06	1.33 / 4.04
Cross-modal w/ reg	0.18 / 0.31	0.32 / 0.61	0.49/ 1.09	0.75 / 1.99
<i>State-of-the-art methods</i>				
DESIRE [11]	- / 0.28	- / 0.67	- / 1.22	- / 2.06
Social-GAN [13]	0.29 / 0.43	0.67 / 1.34	1.26 / 2.94	2.07 / 5.22

Table 2: ADE / FDE is evaluated in *pixels*. The KITTI [49] dataset is used to predict trajectories in frontal view. * denotes the evaluation on relative motion of road agents with respect to the ego-future.

Single- & multi-modal prediction				
Method	1.0 <i>sec</i>	2.0 <i>sec</i>	3.0 <i>sec</i>	4.0 <i>sec</i>
<i>Ours</i>				
w/o cross-modal	4.17 / 7.85	8.22 / 17.68	13.63 / 30.48	19.63 / 44.97
Cross-modal_single	4.17 / 7.35	8.21 / 17.64	13.59 / 30.41	19.59 / 44.92
Cross-modal_multi	3.25 / 5.57	5.71 / 10.74	8.25 / 15.74	11.22 / 24.85
<i>State-of-the-art</i>				
Conv-1D* [20]	24.38 / 44.13	- / -	- / -	- / -
FVL* [21]	17.88 / 37.11	- / -	- / -	- / -
Const-vel [50]	5.88 / 9.42	13.23 / 26.03	22.13 / 45.99	31.90 / 68.03
Social-GAN_single [13]	7.54 / 10.51	13.39 / 23.74	21.37 / 43.82	31.76 / 71.55
Social-GAN_multi [13]	6.96 / 9.58	12.25 / 21.42	19.48 / 39.66	28.89 / 65.02

temporal are similar, the results imply the role of social stimuli for trajectory prediction with the significant improvement at the short-term time steps. We ob-

Table 3: Quantitative results (ADE / FDE) are reported in *meters*. We use the H3D [6] dataset for evaluation in top-down view.

Single- & multi-modal prediction				
Method	1.0 <i>sec</i>	2.0 <i>sec</i>	3.0 <i>sec</i>	4.0 <i>sec</i>
<i>Ours</i>				
Cross-modal_single	0.14 / 0.25	0.27 / 0.54	0.43 / 0.95	0.62 / 1.45
Cross-modal_multi	0.12 / 0.21	0.21 / 0.37	0.30 / 0.61	0.42 / 0.96
<i>State-of-the-art methods</i>				
Const-Vel [50]	0.18 / 0.26	0.34 / 0.60	0.52 / 1.03	0.74 / 1.54
Social-LSTM [10]	0.26 / 0.41	0.49 / 0.92	0.72 / 1.53	1.01 / 2.32
Social-GAN_single [13]	0.27 / 0.37	0.45 / 0.77	0.68 / 1.29	0.94 / 1.91
Social-GAN_multi [13]	0.26 / 0.35	0.44 / 0.72	0.65 / 1.24	0.90 / 1.84
Gated-RN [36]	0.18 / 0.32	0.32 / 0.64	0.49 / 1.03	0.69 / 1.56
Trajectron++ [52]	0.21 / 0.34	0.33 / 0.62	0.46 / 0.93	0.71 / 1.63

Table 4: Our approach is evaluated on ADE / FDE (in *pixels*) using H3D [6]. Note that the absolute motion is captured in frontal view.

Single- & multi-modal prediction				
Method	1.0 <i>sec</i>	2.0 <i>sec</i>	3.0 <i>sec</i>	4.0 <i>sec</i>
<i>Ours</i>				
Cross-modal_single	8.69 / 16.06	16.52 / 33.25	25.68 / 54.91	36.29 / 82.05
Cross-modal_multi	6.62 / 11.36	10.69 / 18.12	14.25 / 24.51	18.22 / 36.92
<i>State-of-the-art</i>				
Const-vel [50]	13.15 / 19.22	24.64 / 44.13	38.18 / 74.75	53.38 / 110.07
Social-GAN_single [13]	12.91 / 17.05	20.57 / 33.53	29.70 / 54.41	40.71 / 84.51
Social-GAN_multi [13]	12.38 / 16.26	19.67 / 31.86	28.30 / 51.55	38.88 / 80.55

serve the impressive error drop by taking all types of stimuli into account (**w/o cross-modal**), which demonstrates the validity of the proposed feature extractor. Lastly, further improvement of the performance is achieved with cross-modal embedding (**Cross-modal single**), particularly at the short-term time steps. We find the reason from the nature of RGB images where the objects/regions closer to the camera are more clearly presented. Consequently, it shows that the model is able to take the complementary features through the proposed cross-modal learning. Additionally, we quantitatively show the efficacy of the proposed regularizer from the multi-modal prediction. Without the proposed regularizer, the improvement of multi-modal sampling (**Cross-modal w/o reg**) over its single-modal prediction (**Cross-modal single**) is minimal. However, the model **Cross-modal w/ reg** highly improves the accuracy generating diverse output responses.

5.3 Quantitative Results

We first compare the performance of the proposed approach with the state-of-the-art methods using KITTI. In Table 1, trajectories of the road agents are

predicted in top-down view. We observe that Gated-RN [36] on ADE and DE-SIRE [11] on FDE achieves higher accuracy, compared to the Social-LSTM [10] and Social-GAN [13]. This is partially because [11,36] uses images to capture scene context, which is also validated from our ablative study. Considering all stimuli, cross-modal embedding, as well as the regularizer, our approach further boost the performance of both single- and multi-modal prediction. We achieve lower ADE and FDE than these competitors at all time steps in top-down view trajectory forecast. Using the same Cross-modal model, we examine the frontal view-based prediction capability in Table 2. Note that Conv-1D [20] and FVL [21] predicts relative motion with respect to the future ego-motion. Their poor performance might be caused by the prediction difficulties with unknown ego-future. Instead, the rest of methods use the absolute motion with ego-compensation. Similar to prediction in top-down view, the proposed method generally shows higher accuracy against others. Interestingly, the error gap between **w/o cross-modal** and **Cross-modal_single** is getting larger for near-future prediction. Our insight for this is that the behavior representations obtained from top-down view would help the model to understand the influences of occlusions behind the agent or obstacle.

We further compare our work with the state-of-the-art methods using the H3D dataset. In top-down view as in Table 3, the method with scene context (Gated-RN [36] and Trajectron++ [52]) shows lower errors than Social-LSTM [10] and Social-GAN [13]. Our explicit modeling of relational interactions between heterogeneous agents, based on three types of stimuli, enables us to encode more discriminative behavior representations against other state-of-the-art methods. Thus, we achieve the lower error rate even with a single sample. The results on ADE / FDE are significantly improved with multi-modal framework with a help with the regularizer. Such lower error rates signify the generation of highly diverse future motions that have acceptable topology in the scene. Subsequently, we evaluate our trajectory prediction framework for the task of frontal view forecast. We observe that the performance of our single-modal prediction model (**Cross-modal_single**) is similar to multi-modal prediction model of Social-GAN. It implies that the prediction capability of the decoder is being at the level of the state-of-the-art. The significant drop of error rate from the model **Cross-modal_multi** further demonstrates the effectiveness of our objective function for optimization.

5.4 Qualitative Results in Top-down View

The heterogeneous agents (*i.e.*, cars, bus, pedestrians, cyclist, etc.) are observed on the left in Fig. 3. On the right, we robustly forecast their future motion by taking advantages of the proposed interaction module and cross-modal embedding framework. In Fig. 4, we illustrate interactive scenarios in the H3D dataset. In between pedestrians, our approach models their motion behaviors and generate socially acceptable trajectories (red-dotted oval in 4a). Also, the interaction between pedestrian and vehicle is captured in 4b (future motion with green and brown). While making turns, our approach models interact between vehicles in



Fig. 3: Highly interactive scenarios in the H3D dataset. (Left) An RGB image captures rich and dense representation, particularly for closer objects. (Right) Predicted trajectories of those traffic agents.

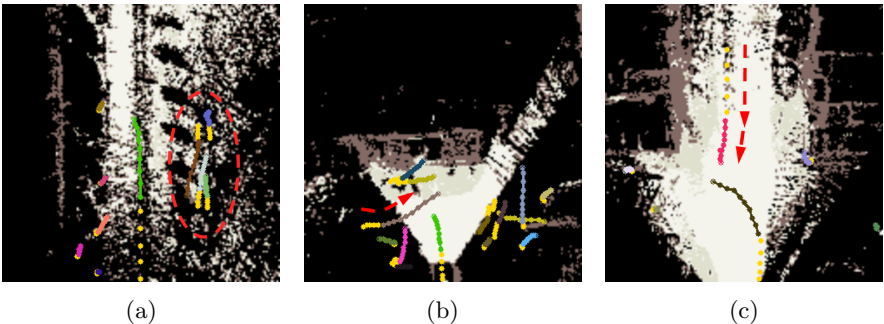


Fig. 4: We visualize the top-1 prediction. (a) human-human interaction on the sidewalk. (b) human-vehicle interaction at the three-way intersection. (c) vehicle-vehicle interaction while turning left.

4c. The on-coming vehicle slows its speed. Therefore, we conclude the proposed interaction module accordingly considers different types of interactions while predicting future motions.

6 Conclusion

We proposed a solution to future trajectory forecast in driving scenarios. Assuming that the multiple sensory data is available for autonomous driving, we chose two exemplary input modalities, LiDAR point clouds for top-down view and RGB images for frontal view trajectories. Our feature encoder first extracts motion behavior of traffic agents considering inertial, environmental, and social stimuli. Such behavior representations obtained from multiple perspectives are then embedded into a single cross-modal latent space using the CVAE-based generative model. Since the conventional optimization of CVAE often suffers from posterior collapse, we designed an auxiliary regularizer to alleviate the problem. As a result, the sampled latent variables generated diverse modes of future trajectories while preventing the performance drop. We analyzed the significance of the proposed approach through the extensive evaluation, improving the performance of the state-of-the-art methods.

Supplementary Material

A Dataset Preprocessing

A.1 Frontal View Input

Segmentation Map Frontal view RGB images (top row in Fig. 5) are used to estimate the semantic labels in the scene. We first run the DeepLab-V2 [9] model trained on the Cityscapes dataset [48] dataset. Then, we leave the background labels with stationary structures (*i.e.*, road, sidewalk, building, etc.) to get the background map as shown in the second row of Fig. 5. For the static stream, we directly use the background map at time $t = t_0 - \tau + 1$ as segmentation input S to the model.

Ego-motion Compensation Note that the trajectories in frontal view are computed from the absolute locations. To compensate the ego-motion for dynamic stream, we make the local coordinates at time $t = t_0 - \tau + 1$ for every trajectory segments (length $\tau + \delta$), and all foreground objects for each trajectory segment are projected into this space as shown in the thrid row of Fig. 5. For this, we conduct the following procedure. First, the point cloud in the world coordinates is projected into the image space to grab the corresponding RGB information. Next, we transform the point cloud to the first frame at time $t = t_0 - \tau + 1$ using GPS/IMU position estimates. Finally, the transformed point cloud is projected into the empty image with previously acquired RGB.

Optical Flow Images Foreground images are generated using the ground truth bounding box in the image space. Then, we go through ego-motion compensation using foreground images with their corresponding point clouds. The outputs (last row in Fig. 5) are used to compute optical flow \mathcal{O} by running TV-L1. The locations of each object is also computed with this procedure. Images have a dimension of 414×125 .

A.2 Top-down View Image

Segmentation Map From each trajectory segment, we grab the segmentation label for the point cloud from the RGB-based background map. Then, the point

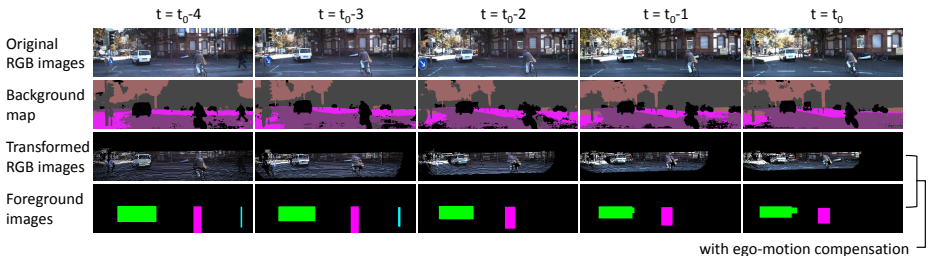


Fig. 5: Frontal view input.

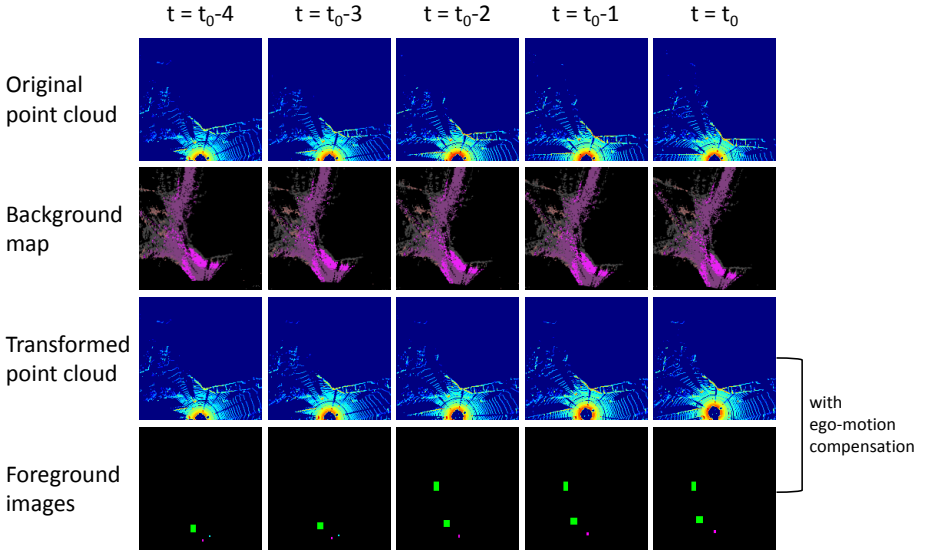


Fig. 6: Top-down view input.

cloud is transformed onto the top-down image space that is discretized with a resolution of 0.5 m as illustrated in the second row of Fig. 6. We use the map at time $t = t_0 - \tau + 1$ as S in top-down view.

Ego-motion Compensation Similar to frontal view images, we first transform each point cloud to the local coordinates at $t = t_0 - \tau + 1$ of the segment using GPS/IMU position estimates. The transformed point clouds are projected into the top-down view image space with a resolution of 0.5 m . The third row of Fig. 6 shows the transformed point clouds from the first row of Fig. 6.

Optical Flow Images The ground truth bounding box of objects are first compensated for ego-motion. Then, they are drawn in the top-down view image space as displayed in the last row of Fig. 6. The final output has a dimension of 160×160 that corresponding to 80 m to the longitudinal direction and $\pm 40\text{ m}$ to the lateral direction.

B Qualitative Results in Frontal View

We additionally show the qualitative results of the proposed method in frontal view using the KITTI [49] dataset. As shown in Fig. 7, our frontal view prediction is based on the absolute locations (with ego-motion compensation) in the local coordinates of the first frame of each trajectory segment. The proposed approach recognizes the road layouts and predict interactive future motions of different types of road agents. Note that we visualize top-1 prediction in this figure.

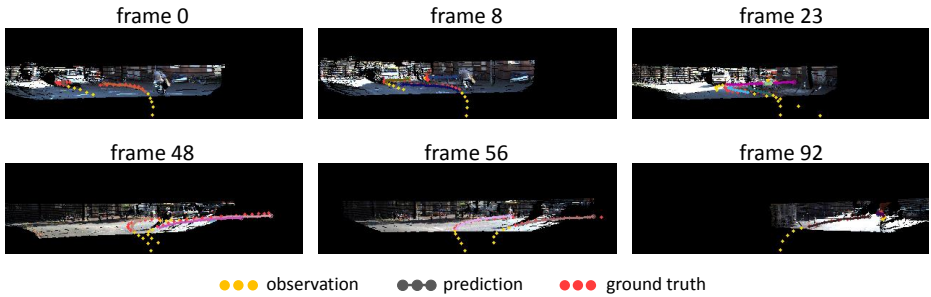


Fig. 7: Additional qualitative results evaluated using KITTI in frontal view.

References

1. Lin, T.Y., Dollár, P., Girshick, R., He, K., Hariharan, B., Belongie, S.: Feature pyramid networks for object detection. In: CVPR. Volume 1. (2017) 4 **1**
2. Dai, J., Qi, H., Xiong, Y., Li, Y., Zhang, G., Hu, H., Wei, Y.: Deformable convolutional networks. In: Proceedings of the IEEE International Conference on Computer Vision. (2017) 764–773 **1**
3. Liu, S., Qi, L., Qin, H., Shi, J., Jia, J.: Path aggregation network for instance segmentation. In: Proceedings of the IEEE Conference on Computer Vision and Pattern Recognition. (2018) 8759–8768 **1**
4. Kim, C., Li, F., Ciptadi, A., Rehg, J.M.: Multiple hypothesis tracking revisited. In: Proceedings of the IEEE International Conference on Computer Vision. (2015) 4696–4704 **1**
5. Bertinetto, L., Valmadre, J., Henriques, J.F., Vedaldi, A., Torr, P.H.: Fully-convolutional siamese networks for object tracking. In: European conference on computer vision, Springer (2016) 850–865 **1**
6. Patil, A., Malla, S., Gang, H., Chen, Y.T.: The h3d dataset for full-surround 3d multi-object detection and tracking in crowded urban scenes. In: 2019 International Conference on Robotics and Automation (ICRA), IEEE (2019) 9552–9557 **1, 9, 10, 12**
7. Zhao, H., Shi, J., Qi, X., Wang, X., Jia, J.: Pyramid scene parsing network. In: IEEE Conf. on Computer Vision and Pattern Recognition (CVPR). (2017) 2881–2890 **1**
8. He, K., Gkioxari, G., Dollár, P., Girshick, R.: Mask r-cnn. In: Computer Vision (ICCV), 2017 IEEE International Conference on, IEEE (2017) 2980–2988 **1**
9. Chen, L.C., Papandreou, G., Kokkinos, I., Murphy, K., Yuille, A.L.: Deeplab: Semantic image segmentation with deep convolutional nets, atrous convolution, and fully connected crfs. IEEE transactions on pattern analysis and machine intelligence **40**(4) (2018) 834–848 **1, 6, 15**
10. Alahi, A., Goel, K., Ramanathan, V., Robicquet, A., Fei-Fei, L., Savarese, S.: Social lstm: Human trajectory prediction in crowded spaces. In: Proceedings of the IEEE Conference on Computer Vision and Pattern Recognition. (2016) 961–971 **1, 4, 11, 12, 13**
11. Lee, N., Choi, W., Vernaza, P., Choy, C.B., Torr, P.H., Chandraker, M.: Desire: Distant future prediction in dynamic scenes with interacting agents. In: Proceed-

- ings of the IEEE Conference on Computer Vision and Pattern Recognition. (2017) 336–345 [1](#), [3](#), [4](#), [10](#), [11](#), [13](#)
12. Su, S., Pyo Hong, J., Shi, J., Soo Park, H.: Predicting behaviors of basketball players from first person videos. In: Proceedings of the IEEE Conference on Computer Vision and Pattern Recognition. (2017) 1501–1510 [2](#)
 13. Gupta, A., Johnson, J., Fei-Fei, L., Savarese, S., Alahi, A.: Social gan: Socially acceptable trajectories with generative adversarial networks. In: IEEE Conference on Computer Vision and Pattern Recognition (CVPR). (2018) [2](#), [4](#), [11](#), [12](#), [13](#)
 14. Hasan, I., Setti, F., Tsesmelis, T., Del Bue, A., Galasso, F., Cristani, M.: Mx-lstm: Mixing tracklets and vislets to jointly forecast trajectories and head poses. In: The IEEE Conference on Computer Vision and Pattern Recognition (CVPR). (June 2018) [2](#)
 15. Xu, Y., Piao, Z., Gao, S.: Encoding crowd interaction with deep neural network for pedestrian trajectory prediction. In: Proceedings of the IEEE Conference on Computer Vision and Pattern Recognition. (2018) 5275–5284 [2](#), [4](#)
 16. Vemula, A., Muelling, K., Oh, J.: Social attention: Modeling attention in human crowds. In: 2018 IEEE International Conference on Robotics and Automation (ICRA), IEEE (2018) 1–7 [2](#), [4](#)
 17. Ma, Y., Zhu, X., Zhang, S., Yang, R., Wang, W., Manocha, D.: Trafficpredict: Trajectory prediction for heterogeneous traffic-agents. (2019) [2](#), [4](#)
 18. Deo, N., Trivedi, M.M.: Multi-modal trajectory prediction of surrounding vehicles with maneuver based lstms. In: 2018 IEEE Intelligent Vehicles Symposium (IV), IEEE (2018) 1179–1184 [2](#), [4](#)
 19. Park, S.H., Kim, B., Kang, C.M., Chung, C.C., Choi, J.W.: Sequence-to-sequence prediction of vehicle trajectory via lstm encoder-decoder architecture. In: 2018 IEEE Intelligent Vehicles Symposium (IV), IEEE (2018) 1672–1678 [2](#), [4](#)
 20. Yagi, T., Mangalam, K., Yonetani, R., Sato, Y.: Future person localization in first-person videos. In: The IEEE Conference on Computer Vision and Pattern Recognition (CVPR). (June 2018) [2](#), [5](#), [11](#), [13](#)
 21. Yao, Y., Xu, M., Choi, C., Crandall, D.J., Atkins, E.M., Dariush, B.: Egocentric vision-based future vehicle localization for intelligent driving assistance systems. In: IEEE International Conference on Robotics and Automation (ICRA), IEEE (2019) [2](#), [3](#), [4](#), [5](#), [10](#), [11](#), [13](#)
 22. Huang, X., McGill, S., Williams, B.C., Fletcher, L., Rosman, G.: Uncertainty-aware driver trajectory prediction at urban intersections. 2019 IEEE International Conference on Robotics and Automation (ICRA) (2019) [2](#), [4](#)
 23. Malla, S., Choi, C.: Nemo: Future object localization using noisy ego priors. arXiv preprint arXiv:1909.08150 (2019) [2](#), [3](#), [4](#)
 24. Rhinehart, N., Kitani, K.M., Vernaza, P.: R2p2: A reparameterized pushforward policy for diverse, precise generative path forecasting. In: Proceedings of the European Conference on Computer Vision (ECCV). (2018) 772–788 [2](#), [3](#), [4](#)
 25. Choi, C., Patil, A., Malla, S.: Drogon: A causal reasoning framework for future trajectory forecast. arXiv preprint arXiv:1908.00024 (2019) [2](#), [3](#), [4](#)
 26. Zeng, W., Luo, W., Suo, S., Sadat, A., Yang, B., Casas, S., Urtasun, R.: End-to-end interpretable neural motion planner. In: Proceedings of the IEEE Conference on Computer Vision and Pattern Recognition. (2019) 8660–8669 [2](#)
 27. Zhao, T., Xu, Y., Monfort, M., Choi, W., Baker, C., Zhao, Y., Wang, Y., Wu, Y.N.: Multi-agent tensor fusion for contextual trajectory prediction. In: Proceedings of the IEEE Conference on Computer Vision and Pattern Recognition. (2019) 12126–12134 [2](#)

28. Rhinehart, N., McAllister, R., Kitani, K., Levine, S.: Precog: Prediction conditioned on goals in visual multi-agent settings. In: Proceedings of the IEEE International Conference on Computer Vision. (2019) 2821–2830 [2](#), [4](#)
29. Chai, Y., Sapp, B., Bansal, M., Anguelov, D.: Multipath: Multiple probabilistic anchor trajectory hypotheses for behavior prediction. arXiv preprint arXiv:1910.05449 (2019) [2](#)
30. Rudenko, A., Palmieri, L., Herman, M., Kitani, K.M., Gavrila, D.M., Arras, K.O.: Human motion trajectory prediction: A survey. arXiv preprint arXiv:1905.06113 (2019) [2](#)
31. Su, S., Peng, C., Shi, J., Choi, C.: Potential field: Interpretable and unified representation for trajectory prediction. arXiv preprint arXiv:1911.07414 (2019) [2](#)
32. Bhattacharyya, A., Fritz, M., Schiele, B.: Long-term on-board prediction of people in traffic scenes under uncertainty. In: Proceedings of the IEEE Conference on Computer Vision and Pattern Recognition. (2018) 4194–4202 [3](#), [4](#)
33. Zhang, P., Ouyang, W., Zhang, P., Xue, J., Zheng, N.: Sr-lstm: State refinement for lstm towards pedestrian trajectory prediction. In: Proceedings of the IEEE Conference on Computer Vision and Pattern Recognition. (2019) 12085–12094 [4](#)
34. Xue, H., Huynh, D.Q., Reynolds, M.: Ss-lstm: A hierarchical lstm model for pedestrian trajectory prediction. In: 2018 IEEE Winter Conference on Applications of Computer Vision (WACV), IEEE (2018) 1186–1194 [4](#)
35. Kosaraju, V., Sadeghian, A., Martín-Martín, R., Reid, I., Rezatofighi, H., Savarese, S.: Social-bigat: Multimodal trajectory forecasting using bicycle-gan and graph attention networks. In: Advances in Neural Information Processing Systems. (2019) 137–146 [4](#)
36. Choi, C., Dariush, B.: Looking to relations to future trajectory forecast. In: Computer Vision (ICCV), 2019 IEEE International Conference on, IEEE (2019) [4](#), [8](#), [11](#), [12](#), [13](#)
37. Li, J., Ma, H., Tomizuka, M.: Interaction-aware multi-agent tracking and probabilistic behavior prediction via adversarial learning. In: 2019 IEEE International Conference on Robotics and Automation (ICRA), IEEE (2019) [4](#)
38. Li, J., Ma, H., Tomizuka, M.: Conditional generative neural system for probabilistic trajectory prediction. In: 2019 IEEE Conference on Robotics and Systems (IROS). (2019) [4](#)
39. Ngiam, J., Khosla, A., Kim, M., Nam, J., Lee, H., Ng, A.Y.: Multimodal deep learning. In: Proceedings of the 28th international conference on machine learning (ICML-11). (2011) 689–696 [4](#)
40. Jain, A., Singh, A., Koppula, H.S., Soh, S., Saxena, A.: Recurrent neural networks for driver activity anticipation via sensory-fusion architecture. In: 2016 IEEE International Conference on Robotics and Automation (ICRA), IEEE (2016) 3118–3125 [4](#)
41. Yang, X., Molchanov, P., Kautz, J.: Multilayer and multimodal fusion of deep neural networks for video classification. In: Proceedings of the 24th ACM international conference on multimedia, ACM (2016) 978–987 [4](#)
42. Gupta, S., Hoffman, J., Malik, J.: Cross modal distillation for supervision transfer. In: Proceedings of the IEEE conference on computer vision and pattern recognition. (2016) 2827–2836 [4](#)
43. Choi, C., Kim, S., Ramani, K.: Learning hand articulations by hallucinating heat distribution. In: Proceedings of the IEEE International Conference on Computer Vision. (2017) 3104–3113 [4](#)

44. Yi, D., Lei, Z., Li, S.Z.: Shared representation learning for heterogenous face recognition. In: 2015 11th IEEE international conference and workshops on automatic face and gesture recognition (FG). Volume 1., IEEE (2015) 1–7 [4](#)
45. Peng, Y., Huang, X., Qi, J.: Cross-media shared representation by hierarchical learning with multiple deep networks. In: IJCAI. (2016) 3846–3853 [4](#)
46. Aytar, Y., Castrejon, L., Vondrick, C., Pirsivash, H., Torralba, A.: Cross-modal scene networks. *IEEE transactions on pattern analysis and machine intelligence* **40**(10) (2017) 2303–2314 [4](#)
47. Zach, C., Pock, T., Bischof, H.: A duality based approach for realtime tv-l 1 optical flow. In: Joint pattern recognition symposium, Springer (2007) 214–223 [6](#)
48. Cordts, M., Omran, M., Ramos, S., Rehfeld, T., Enzweiler, M., Benenson, R., Franke, U., Roth, S., Schiele, B.: The cityscapes dataset for semantic urban scene understanding. In: Proceedings of the IEEE conference on computer vision and pattern recognition. (2016) 3213–3223 [6](#), [15](#)
49. Geiger, A., Lenz, P., Stiller, C., Urtasun, R.: Vision meets robotics: The kitti dataset. *The International Journal of Robotics Research* **32**(11) (2013) 1231–1237 [9](#), [11](#), [16](#)
50. Schöller, C., Aravantinos, V., Lay, F., Knoll, A.: What the constant velocity model can teach us about pedestrian motion prediction. In: arXiv: 1903.07933. (2019) [11](#), [12](#)
51. Robicquet, A., Sadeghian, A., Alahi, A., Savarese, S.: Learning social etiquette: Human trajectory understanding in crowded scenes. In: European conference on computer vision, Springer (2016) 549–565 [11](#)
52. Salzmann, T., Ivanovic, B., Chakravarty, P., Pavone, M.: Trajectron++: Multi-agent generative trajectory forecasting with heterogeneous data for control. arXiv preprint arXiv:2001.03093 (2020) [12](#), [13](#)